Systematic study of neutron-rich rare isotope production in peripheral heavy-ion collisions below the Fermi energy

P. N. Fountas,[1] G. A. Souliotis,[1,*] M. Veselsky,[2] and A. Bonasera[3,4]

[1]*Laboratory of Physical Chemistry, Department of Chemistry, National and Kapodistrian University of Athens, Athens 15771, Greece*

[2]*Institute of Physics, Slovak Academy of Sciences, Bratislava 84511, Slovakia*

[3]*Cyclotron Institute, Texas A&M University, College Station, Texas 77843, USA*

[4]*Laboratori Nazionali del Sud, INFN, via Santa Sofia 62, I-95123 Catania, Italy*

(Received 25 August 2014; published 15 December 2014)

Detailed calculations of the yields of projectilelike fragments (with focus on the neutron-rich isotopes) are presented for the interaction of ^{86}Kr (15 MeV/nucleon) with ^{64}Ni, ^{58}Ni, and ^{124}Sn, ^{112}Sn, as well as ^{86}Kr (25 MeV/nucleon) with ^{124}Sn and compared with our recently published experimental data for these reactions. The calculations are based on a two-step approach: the dynamical stage of the collision was described with the microscopic constrained molecular dynamics (CoMD) model, as well as the phenomenological deep-inelastic transfer (DIT) model and its modified (DITm) version. The deexcitation of the hot projectile fragments was performed with the statistical multifragmentation model (SMM) and the binary-decay model GEMINI, which provided nearly similar results for the neutron-rich products from the reactions studied. An overall good agreement of the calculations with the experimental results, especially for near-projectile isotopes was observed using both the CoMD model and the DITm model for the dynamical stage. The successful description of the production of neutron-rich isotopes with the CoMD model is of particular importance, due to the predictive power of the microscopic approach that essentially does not depend on the reaction dynamics. Our studies to date suggest that peripheral heavy-ion collisions at this energy range (i.e., well above the Coulomb barrier, but below the Fermi energy), if induced by neutron-rich rare-isotope beams of adequate intensity may offer a unique route to access extremely neutron-rich rare isotopes toward the astrophysical r-process path and the presently uncharted neutron drip line.

DOI: 10.1103/PhysRevC.90.064613 PACS number(s): 25.70.Hi, 25.70.Lm

I. INTRODUCTION

During nearly a century since the dawn of nuclear physics, approximately one half of the estimated 7000 bound nuclei have been produced and investigated [1–3]. The β-stable nuclei occurring in nature are only a small fraction of the nuclei between the lines of proton and neutron stability (the so-called proton and neutron drip lines, respectively). Nuclei away from the line of β stability are, of course, not present in nature and, to be investigated, they need to be prepared in laboratory using appropriate nuclear reactions and separation techniques [4]. Most of the known β-unstable nuclei are proton-rich nuclei produced using compound nucleus and spallation reactions. On the neutron-rich side, exotic nuclei have been explored only in a few regions. For that reason, access and study of new regions of the nuclear landscape toward the neutron drip line is currently one of the major efforts in nuclear physics research. Investigation of very neutron-rich nuclei offers the possibility to understand aspects of nuclear structure with increasing neutron-to-proton ratio (N/Z) [5] and to elucidate important nucleosynthesis processes [6], most notably the rapid neutron-capture process (r process) [7,8]. Furthermore, reactions induced by neutron-rich nuclei can provide information on the isospin dependence of the effective nucleon-nucleon interaction and, thus, shed light on the equation of state [9–13] of asymmetric nuclear matter, which is an important ingredient of the physics of supernova and neutron stars [14–16].

For the aforementioned reasons, the efficient production of very neutron-rich nuclides is a central issue in current and future rare isotope beam facilities (see, e.g., Refs. [17–26]) and, at the same time, the search for new and efficient production approaches is of great importance. Neutron-rich nuclides are mainly produced by spallation, fission, and projectile fragmentation [4,27]. Spallation is an important mechanism to produce rare isotopes for ISOL-type techniques [28]. Projectile fission has proved to be an effective production approach mainly in the region of light and heavy fission fragments (see, e.g., Refs. [29–31] for recent efforts on ^{238}U projectile fission). Finally, projectile fragmentation offers a very successful approach to produce a broad range of exotic nuclei at beam energies above 100 MeV/nucleon (see, e.g., Refs. [32–36] for recent work on projectile fragmentation). This approach is, nevertheless, based on the fact that optimum neutron excess in the fragments is achieved by stripping the maximum possible number of protons and no neutrons (or a minimum possible number of neutrons).

To reach a high neutron excess in the products, apart from proton stripping, it is important to capture neutrons from the target. Such a possibility is offered by reactions of nucleon exchange at beam energies from the Coulomb barrier [37,38] to the Fermi energy (20–40 MeV/nucleon) [39,40]. Detailed experimental data in this broad energy range remain scarce, mainly due to the complicated procedure of isotope identification and separation [38,41,42]. We note that in multinucleon transfer and deep-inelastic reactions near the

*Corresponding author: soulioti@chem.uoa.gr

Coulomb barrier [38], the low velocities of the fragments and the wide angular and ionic charge state distributions of the projectile fragments may limit the collection efficiency for the most neutron-rich products.

The reactions in the Fermi energy regime [43] combine the advantages of both low-energy (i.e., near and above the Coulomb barrier) and high-energy (i.e., above 100 MeV/nucleon) reactions. At this energy, the synergy of the projectile and the target results in broad N/Z distributions of the fragments, whereas the velocities are high enough to allow efficient in-flight collection and separation of the projectile fragments.

Our initial experimental studies of projectile fragments from 25 MeV/nucleon reactions of ^{86}Kr on ^{64}Ni [39] and ^{124}Sn [40] indicated substantial production of neutron-rich nuclei. The production mechanism was described by a deep-inelastic transfer model [44] and a modified version of it [45]. In these reactions, neutron-rich projectile fragments with up to 4–5 neutrons picked up from the target (along with the usual proton-removal products) were observed, demonstrating the important role of the target in the production mechanism. Motivated by recent developments in several facilities that will offer either intense primary beams [20,23] at this energy range or reaccelerated rare isotope beams [19,20,23,24,26], we continued our experimental studies with detailed measurements at 15 MeV/nucleon that were recently published in Ref. [46]. In these measurements, neutron pick-up isotopes (with up to 6–8 neutrons picked up from the target) were observed with large cross sections. Interestingly, the data at 15 MeV/nucleon show larger production cross sections of neutron-rich isotopes very close to the projectile, relative to the corresponding data at 25 MeV/nucleon. This additional enhancement in the cross sections is associated with very peripheral collisions and longer interaction times of the ^{86}Kr projectile with the neutron-rich targets, as well as lower excitation energies of the primary neutron-rich projectile residues.

To advance our understanding of the evolution of the reaction mechanisms at this energy range, we sought for a reliable model framework that, on the one hand be able to describe the experimental data obtained so far and, on the other hand allow dependable predictions of rates of neutron-rich rare isotopes in various production and separation schemes employing such reactions. The latter possibility is crucial for the selection and design of the proper separator configuration (see, e.g., Refs. [47–50]) and the optimum projectile/target combinations (and the appropriate target thickness) for efficient production, collection, and separation of very neutron-rich nuclei.

The work presented in this paper proceeds along these lines. The structure of the paper is as follows. In Sec. II, a short overview of our previous experimental measurements at 15 MeV/nucleon is given. In Sec. III, a description of the theoretical model framework is presented. Two dynamical models were used: the phenomenological deep-inelastic transfer (DIT) model and the microscopic constrained molecular dynamics (CoMD) model. In Sec. IV, we present a systematic comparison of the production cross section calculations with the experimental data. Furthermore, we present calculated production cross sections and rates of neutron-rich nuclei using a radioactive beam of ^{92}Kr at 15 MeV/nucleon interacting with ^{64}Ni. Finally, a discussion and conclusions follow in Sec. V.

II. OUTLINE OF EXPERIMENTAL METHODS AND DATA

A detailed presentation of the experimental results of the 15 MeV/nucleon ^{86}Kr data is published in Ref. [46]. In that paper, the mass spectrometric measurements of production cross sections of neutron-rich projectile fragments from the reactions of a 15 MeV/nucleon ^{86}Kr beam with ^{64}Ni, ^{58}Ni, and ^{124}Sn, ^{112}Sn targets are given. We also note that the experimental results of the 25 MeV/nucleon ^{86}Kr reactions and the relevant procedures are described in detail in our articles [39–42]. We briefly mention that the use of the high-resolution recoil separator MARS [51] in combination with standard $B\rho$-ΔE-E (magnetic rigidity, energy-loss, residual-energy) and time-of-flight techniques provided high-resolution information on the atomic number Z, the ionic charge q, the mass number A, and the velocity distributions of the projectile fragments. Summation over the ionic charge q provided the yield distributions with respect to Z, A, and velocity from which production cross sections were extracted. The measurements were performed inside the grazing angles of the corresponding reactions in a wide $B\rho$ window (via a series of successive magnetic rigidity settings of the separator) that enabled efficient collection of projectilelike residues produced in a broad range of energy damping, from quasielastic to deep-inelastic collisions. Specifically, in the 15 MeV/nucleon ^{86}Kr measurements, the beam hit the target first at 4° and, subsequently at 7.4° and the projectile fragments were collected in the polar angular ranges of 2.2°–5.8° and 5.6°–9.2°, respectively. The total production cross section of each fragment was obtained by appropriate combination and normalization of the individual (differential) cross section measurements at the two angular ranges as explained in Ref. [46].

III. BRIEF DESCRIPTION OF THEORETICAL MODELS

The calculations performed in this work are based on the usual two-stage approach of heavy-ion collisions. The dynamical stage of the collision was described with two models: the phenomenological deep-inelastic transfer (DIT) model [44] and the microscopic constrained molecular dynamics (CoMD) model. For peripheral and semiperipheral collisions, the dynamical stage of the collision leads essentially to an excited projectilelike fragment (quasiprojectile) and an excited targetlike fragment (quasitarget). In the second stage, the resulting excited projectilelike fragments were deexcited with two codes: the binary-decay code GEMINI and the statistical multifragmentation model (SMM). We briefly describe the physical basis of the above dynamical and statistical codes in the following.

A. Deep-inelastic transfer (DIT) model

The phenomenological deep-inelastic transfer (DIT) model implemented by Tassan-Got [44] simulates stochastic nucleon exchange in peripheral and semiperipheral collisions. In the DIT model, the projectile and the target, assumed to be

spherical, approach each other along Coulomb trajectories until they are within the range of the nuclear interaction. At this point the system is represented as two Fermi gases in contact. A window opens in the internuclear potential and stochastic transfer of nucleons may occur. The direction and type of transfer are decided by random drawing based on transfer probabilities. The transfer probabilities are calculated via a phase-space integral that accounts for Pauli blocking and involves a phase-space flux term, the barrier penetrability and the occupation probabilities. The nucleon transfer produces a variation in mass, charge, excitation energy and spin of the interacting nuclei. After the interaction, the primary projectilelike fragment and targetlike fragment are excited and follow Coulomb trajectories. We point out that in DIT, the exchange of nucleons is assumed to be the only source of energy dissipation. Nucleon-nucleon collisions (mostly blocked by the Pauli principle for lower-energy collisions) are not explicitly taken into account in the model. The calculations are performed for a wide range of impact parameters from very peripheral to semiperipheral collisions. The DIT model, that we already employed for the description of the 25 MeV/nucleon ^{86}Kr data [39,40] as mentioned in the introduction, has been successfully used in a number of other studies at Fermi energies (e.g., [52–55]) and is able to describe correctly the N/Z, the excitation energy and kinematic properties of excited projectilelike (and targetlike) residues emerging after the peripheral heavy-ion collision. In addition, the DIT code was employed to describe lower-energy data [56]. In that study, a modification of the nuclear profiles was necessary implying an extended neck between the projectile and the target during their interaction time.

However, as observed in Refs. [39,40], the standard DIT code was not able to properly describe the production cross sections of the neutron-rich fragments in our 25 MeV/nucleon studies. As a first step toward improvements, a modification of the transfer probabilities was introduced in Refs. [40] based on externally calculated neutron and proton density distributions of the reaction partners. Subsequently, an empirical parametrization of the neutron skin of the reaction partners based on neutron and proton separation energies was introduced into the code and was properly taken into account in the nucleon transfer probability. This version of the DIT code [45], that we call modified DIT (DITm), will be used in the present work, along with the standard DIT model.

B. Constrained molecular dynamics (CoMD) model

The microscopic dynamical model employed in this work is the constrained molecular dynamics (CoMD) model of Bonasera and Papa designed for reaction-dynamics studies near and below the Fermi energy [57,58]. Following the general approach of quantum molecular dynamics (QMD) models [59], in the CoMD code nucleons are described as localized Gaussian wave packets. The wave function of the N-body nuclear system is assumed to be the product of these single-particle wave functions. With the Gaussian description, the N-body time-dependent Schrödinger equation leads to (classical) Hamilton's equations of motion for the centroids of the nucleon wave packets. The potential part of the Hamiltonian consists of a Skyrme-like effective interaction and a surface term. The isoscalar part of the effective interaction corresponds to a nuclear matter compressibility of $K = 200$ (soft EOS) or $K = 380$ (stiff EOS). For the isovector part, several forms of the density dependence of the nucleon-nucleon symmetry potential are implemented. Two of them were used in the present work, that we named as the standard potential and the asy-soft potential. These forms correspond to a dependence of the symmetry potential on the 1 and the $1/2$ power of the density, respectively (see Ref. [60] and references therein). We note that in the CoMD model, while not explicitly implementing antisymmetrization of the N-body wave function, a constraint in the phase space occupation for each nucleon is imposed, effectively restoring the Pauli principle at each time step of the (classical) evolution of the system. This constraint restores in an approximate way the fermionic nature of the nucleon motion in the interacting nuclei. The short-range (repulsive) nucleon-nucleon interactions are described as individual nucleon-nucleon collisions governed by the nucleon-nucleon scattering cross section, the available phase space and the Pauli principle, as usually implemented in transport codes. The present CoMD version fully preserves the total angular momentum (along with linear momentum and energy) [58], features that are critical for the accurate description of observables from heavy-ion collisions.

In the present calculations, the CoMD code with its standard parameters was used. The soft density-dependent isoscalar potential was used (corresponding to a compressibility $K = 200$ for symmetric nuclear matter). The calculations were performed with either the standard or the asy-soft symmetry potential and lead to nearly identical results for peripheral collisions. Thus, results with only the standard symmetry potential will be shown in the following figures.

We note that the ground-state configurations of the projectile and the target nuclei were obtained with a simulated annealing approach and were tested for stability for long times (1500–2000 fm/c). These configurations were used in the CoMD code for the subsequent collision simulations. As with the DIT model, the CoMD calculations were performed in a wide range of impact parameters covering from peripheral to semiperipheral collisions.

The CoMD calculations were stopped at $t = 300$fm/c and the characteristics of the produced excited primary projectile residues (quasiprojectiles) were determined with the fragment-recognition routine of CoMD. In the calculations of this work, the excitation energy of the primary projectile residues was determined from the difference of their binding energy as given by the CoMD calculation at $t = 300$fm/c and the corresponding binding energies of the ground-state nuclei taken from mass tables [61]. We have previously investigated the issues of the excitation energy determination [62] using the above approach and we think that we can obtain a reliable estimate of the excitation energies of the quasiprojectiles in our calculations. However, an overestimation of the yields of fragments further from the projectile was observed in the 15 MeV/nucleon reactions with the neutron-rich targets (see below) that may be due to a possible underestimation of the excitation energy of these products. Further investigation of issues related to the excitation energy determination is necessary employing

self-consistently calculated CoMD values of the ground-state binding energies of all the involved fragments, thus avoiding the use of binding energies from mass tables. This is a topic for future research.

C. Models for the deexcitation stage

To describe the deexcitation of the hot projectilelike residues emerging from the dynamical stage, we implemented two different models: the binary-decay code GEMINI [63] and the statistical multifragmentation model SMM [64].

The statistical deexcitation code GEMINI of Charity [63,65] uses Monte Carlo techniques and the Hauser-Feshbach formalism to calculate the probabilities for fragment emission with $Z < 2$. Heavier fragment emission probabilities are calculated via the transition state formalism of Moretto [66]. Within this model, the final partition of products is generated by a succession of fragment emissions (binary decays). In the calculations, we used essentially the parameter set recommended by the author, featuring Lestone's temperature-dependent level density parameter [67], a fading of shell corrections with excitation energy and the option of intermediate-mass fragment (IMF) emission. We mention that this parameter set proved successful in our previous work for the 25 MeV/nucleon reactions ^{86}Kr + ^{64}Ni,^{124}Sn [39,40].

Alternative to the binary-decay scenario of deexcitation is the model of statistical multifragmentation, where the fragment partition is generated at once in the so-called freeze-out configuration. In this work, we use the multifragmentation code SMM of Botvina [64,68–70]. In this code, thermally equilibrated partitions of hot fragments are generated in the hot stage, which is followed by propagation of fragments in their mutual Coulomb field and secondary deexcitation of the hot fragments flying in their asymptotic directions. We point out that for low-excitation energy events ($E^* < 1$ MeV/nucleon) of relevance to the production of very neutron-rich nuclei, the SMM code can describe adequately [56] the deexcitation process as a cascade of emissions of neutrons and light charged particles, using the Weisskopf-Ewing model of statistical evaporation.

D. Comments on the DIT and CoMD models

Concluding this section on the theoretical models, we wish to provide some additional comments on the physical basis of the two models used for the description of the dynamical stage. We stress that the DIT model is a phenomenological nucleon-exchange model with empirical parameters carefully chosen to describe peripheral reactions near the Fermi energy. On the other hand, the CoMD model is a fully microscopic (albeit semiclassical) N-body model of the collisions employing empirical interactions among the nucleons that have been adjusted to describe the known static properties of nuclei (i.e., radii, masses, etc.) [57]. As such, the code has essentially no adjustable parameters that depend on the dynamics to be described. Furthermore, the CoMD model, at variance with mean-field models, naturally takes into account nucleon-nucleon correlations that are of vital importance for the description of observables involving fluctuations, as for example the nucleon transport in peripheral heavy-ion collisions as in this work. We mention that multinucleon transfer in reactions near the Coulomb barrier has been successfully described microscopically by the fully quantal time-dependent Hartree-Fock (TDHF) approach (see, e.g., Ref. [71] and references therein), which is, of course, a mean-field (one-body) approach, and, thus, not appropriate for energies well above the Coulomb barrier. For the above reasons, we believe that the microscopic CoMD model provides an especially valuable theoretical framework for the description of the present reactions. Moreover, the CoMD may be trusted when applied to situations where no experimental data are available, especially in reactions with neutron-rich rare isotope beams, as will be discussed in the following.

IV. COMPARISON OF MODEL CALCULATIONS WITH DATA

In this section we present a systematic comparison of the calculated production cross sections of projectilelike fragments from the ^{86}Kr-induced reactions employing the model frameworks discussed above with our published experimental data mainly at 15 MeV/nucleon [46] and also at 25 MeV/nucleon [40]. Furthermore, we present calculated production cross sections and rates of neutron-rich nuclei using a radioactive beam of ^{92}Kr at 15 MeV/nucleon interacting with a ^{64}Ni target.

A. Reaction ^{86}Kr(15 MeV/nucleon)+^{64}Ni

In Fig. 1 we present a comparison of calculated mass distributions of projectilelike fragments with $Z = 35$–30 from the reaction ^{86}Kr(15 MeV/nucleon)+^{64}Ni with our experimental data [46]. The calculations were performed with the CoMD code [solid (red) line], the modified DIT (DITm) code [dotted (blue) line], and the standard DIT code [dashed (green) line]. In all three calculations, the SMM code was used for the deexcitation stage.

Starting our discussion with the standard DIT code, we observe that the results of the code employed at this energy are not satisfactory, especially on the neutron-rich side. Similar observations were made in our previous studies at 25 MeV/nucleon [39,40] where DIT was followed by GEMINI. In Fig. 1, the modified DIT (DITm) code, in contrast to the standard DIT code, appears to describe the experimental data rather adequately on the neutron-rich side, especially for near-projectile fragments. We remind that in the modified version of DIT, according to our recent work [45], the effect of the neutron-rich nuclear surface on the transfer probability is empirically taken into account.

Finally, in Fig. 1, we observe that the results of the CoMD calculations are in overall agreement with the experimental data especially for the isotopes close to the projectile, i.e., with $Z = 35$–32. It is very interesting to observe that the microscopic CoMD model is able to adequately describe the rare neutron-rich products from this reaction, which are, of course, the nuclides of our main interest. These nuclides come from the projectile nucleus following proton stripping and neutron pickup from the target nucleus.

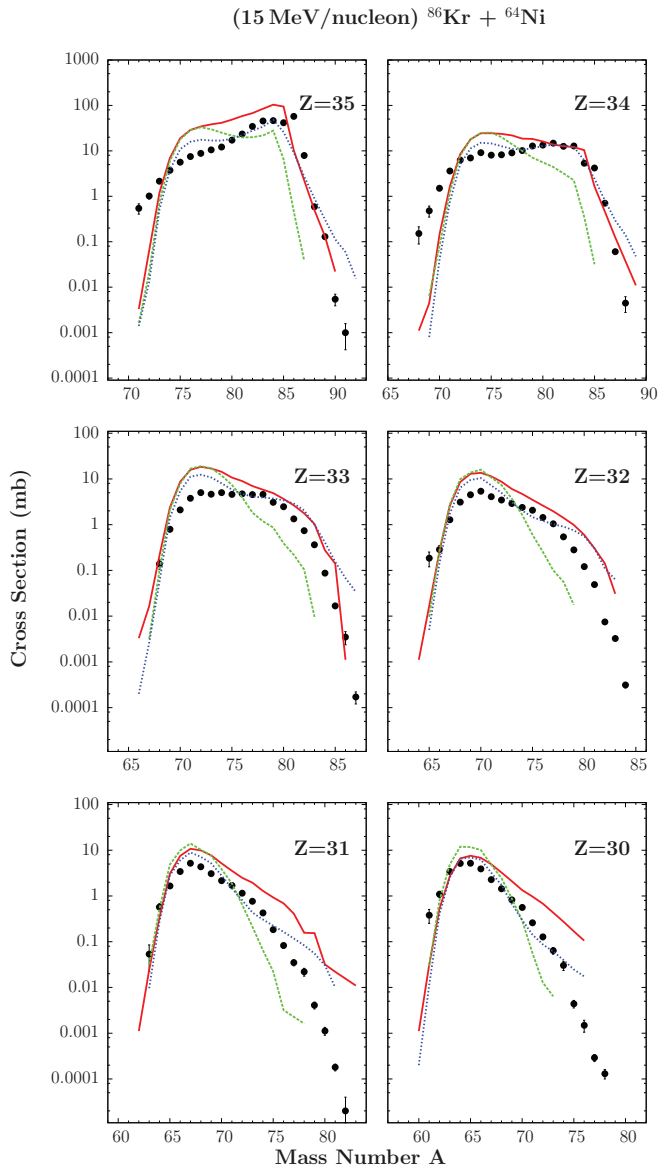

FIG. 1. (Color online) Comparison of calculated mass distributions (lines) of projectilelike fragments with $Z = 35$–30 from the reaction ^{86}Kr(15 MeV/nucleon)+^{64}Ni with the experimental data (closed points) of Ref. [46]. The calculations are: CoMD/SMM [solid (red) line], DITm/SMM [dotted (blue) line], and DIT/SMM [dashed (green) line].

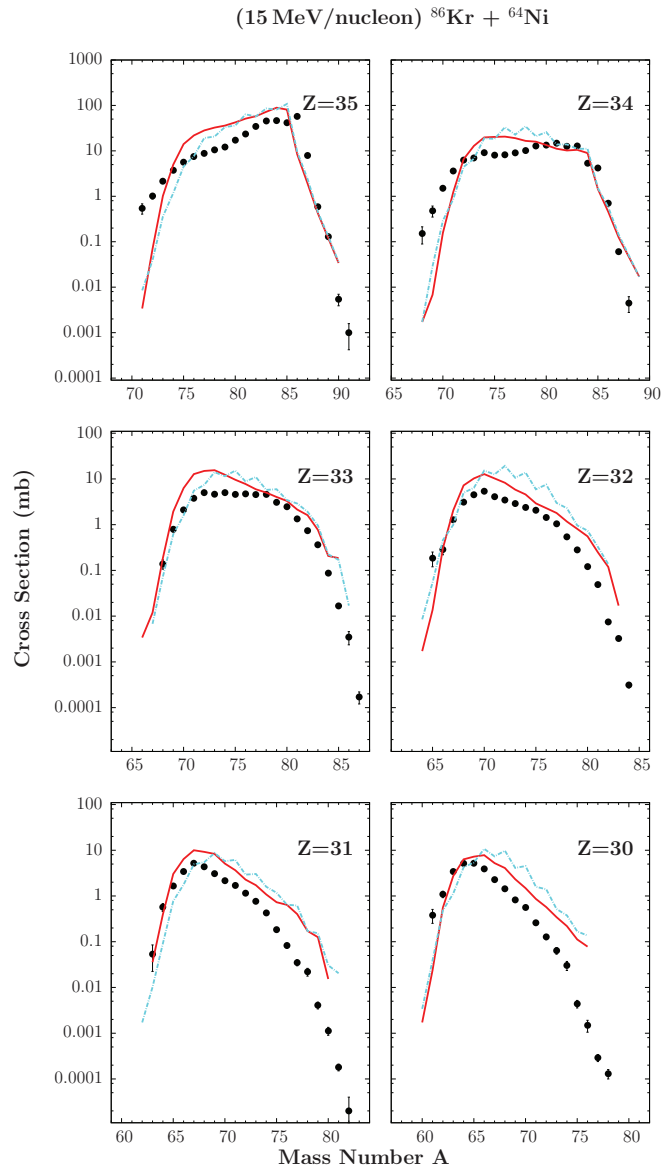

FIG. 2. (Color online) Comparison of calculated mass distributions (lines) of projectilelike fragments with $Z = 35$–30 from the reaction ^{86}Kr(15 MeV/nucleon)+^{64}Ni with the experimental data (closed points) of Ref. [46]. The calculations are: CoMD/SMM [solid (red) line] and CoMD/GEMINI [dash-dotted (light-blue) line].

However, an overestimation of the CoMD yields of fragments further from the projectile, i.e., $Z = 31,30$ is observed in Fig. 1, which we think is due to a possible underestimation of the excitation energy of these products. As we mentioned above, further investigation of the excitation energy determination is necessary. Furthermore, comparing the results of CoMD and DITm, we note that both codes are able to adequately describe the neutron pick-up products for isotopes near the projectile (i.e., $Z = 35,34$).

We now continue with a comparison of the results of the CoMD code followed by the two deexcitation codes: SMM and GEMINI. In Fig. 2 we compare these calculations of the mass distributions of projectilelike fragments with $Z = 35$–30 from the reaction ^{86}Kr(15 MeV/nucleon)+^{64}Ni with the data [46]. The CoMD/SMM calculations are shown by the solid (red) lines and the CoMD/GEMINI calculations by the dash-dotted (light-blue) lines. We observe that the results of the two deexcitation codes are similar and, as we discussed above, the CoMD/SMM and CoMD/GEMINI calculations are in reasonable agreement with the experimental data, especially for the isotopes close to the projectile.

Subsequently, we present the results of the CoMD calculations for transprojectiles residues. In Fig. 3, the calculations of the CoMD model combined with SMM [solid (red) line] and GEMINI [dash-dotted (light-blue) line] are compared with the experimental mass distributions for $Z = 39$–36 from

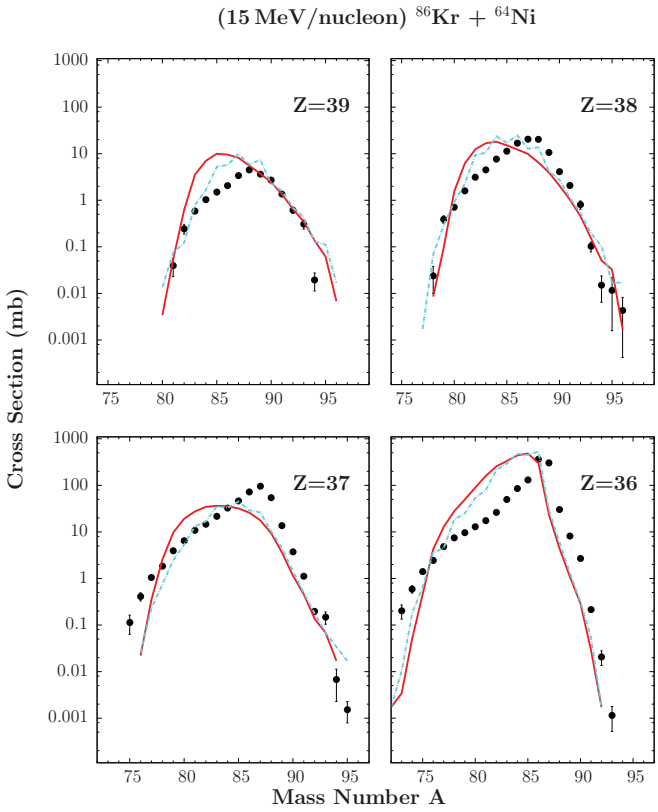

FIG. 3. (Color online) Comparison of calculated mass distributions (lines) of projectilelike fragments with $Z = 39$–36 from the reaction ^{86}Kr(15 MeV/nucleon)+^{64}Ni with the experimental data (closed points) of Ref. [46]. The calculations are: CoMD/SMM [solid (red) line] and CoMD/GEMINI [dash-dotted (light-blue) line].

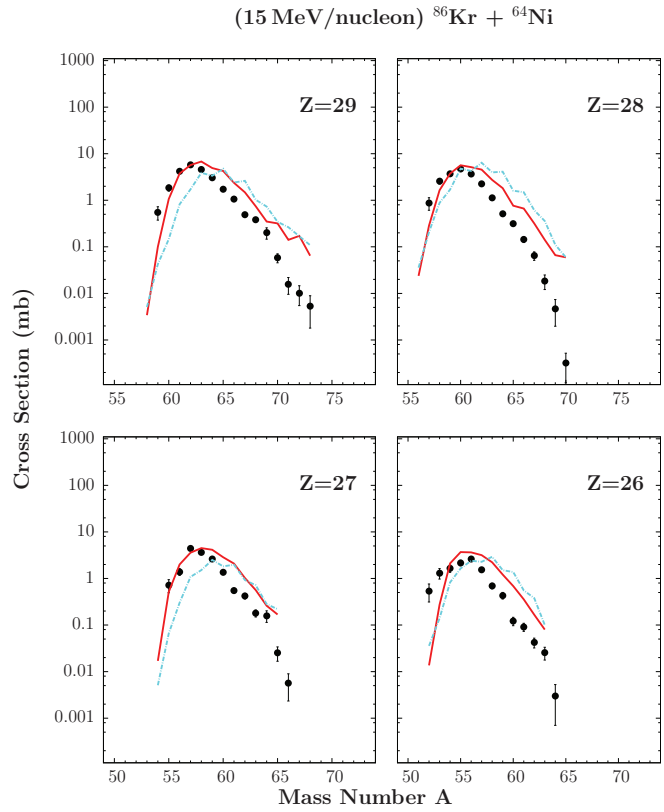

FIG. 4. (Color online) Comparison of calculated mass distributions (lines) of projectilelike fragments with $Z = 29$–26 from the reaction ^{86}Kr(15 MeV/nucleon)+^{64}Ni with the experimental data (closed points) of Ref. [46]. The calculations are: CoMD/SMM [solid (red) line] and CoMD/GEMINI [dash-dotted (light-blue) line].

^{86}Kr(15 MeV/nucleon)+^{64}Ni. We observe that CoMD again is able to describe properly the neutron-rich products of these isotopes. A fair agreement with the experimental results is also obtained for the isotopes that are further below projectile, as seen in Fig. 4. Similar conclusions pertain to the results of the DITm model for products above the projectile as well as further below the projectile, which are not presented in the paper. Thus both dynamical codes, the microscopic CoMD and the phenomenological DITm, combined with either of the two deexcitation codes SMM and GEMINI, as mentioned before, can describe the products of multinucleon transfer at this beam energy in a rather satisfactory manner.

B. Reaction ^{86}Kr(15 MeV/nucleon)+^{124}Sn

Furthermore, we discuss the predictions of CoMD, DITm, and DIT followed by SMM for the ^{86}Kr-induced reaction with the heavier neutron-rich target ^{124}Sn. In Fig. 5, the experimental mass distributions of projectilelike fragments with $Z = 35$–30 from ^{86}Kr(15 MeV/nucleon)+^{124}Sn [46] are compared to the results of the CoMD/SMM [solid (red) line], DITm/SMM [dotted (blue) line] and DIT/SMM [dashed (green) line].

Conclusions similar to the case of ^{86}Kr +^{64} Ni (Fig. 1) follow from this comparison: in contrast to the standard DIT, the DITm code performs well for near-projectile isotopes. Also, we see an overall satisfactory agreement of the CoMD calculations with the experimental results. The disagreement seen for $Z = 35$ and $A = 83$–85 is mainly due to the fact that in the experimental data for these nuclides we had a substantial background of elastically scattered beam, which had to be removed via our data analysis procedures [46]. Again we notice that the neutron-rich products are described well using both the microscopic CoMD model and the phenomenological DITm model combined with SMM. (We mention that results of similar quality are obtained if we use GEMINI for the deexcitation.)

C. Reactions ^{86}Kr(15 MeV/nucleon)+^{58}Ni, ^{112}Sn

After examining the interaction of ^{86}Kr with the neutron-rich ^{64}Ni and ^{124}Sn targets, which are the targets of choice for the efficient production of the most neutron-rich nuclides, we continue our discussion with the ^{86}Kr-induced reactions on the neutron-deficient ^{58}Ni and ^{112}Sn targets. For these reactions, we show representative results with the dynamical codes CoMD, DITm, and DIT followed by SMM deexcitation (as the results with the GEMINI deexcitation are essentially similar). In Fig. 6, the calculations CoMD/SMM [solid (red) line], DITm/SMM [dotted (blue) line], and DIT/SMM [dashed (green) line] for projectilelike fragments

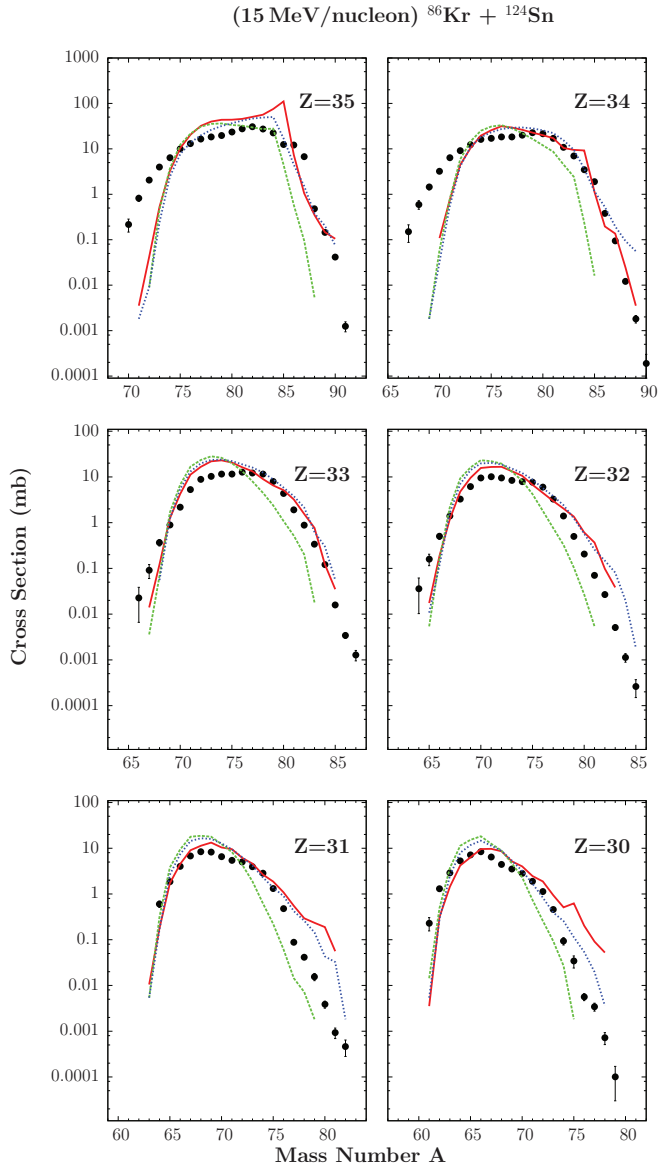

FIG. 5. (Color online) Comparison of calculated mass distributions (lines) of projectilelike fragments with $Z = 35$–30 from the reaction ^{86}Kr(15 MeV/nucleon)+^{124}Sn with the experimental data (closed points) of Ref. [46]. The calculations are: CoMD/SMM [solid (red) line], DITm/SMM [dotted (blue) line], and DIT/SMM [dashed (green) line].

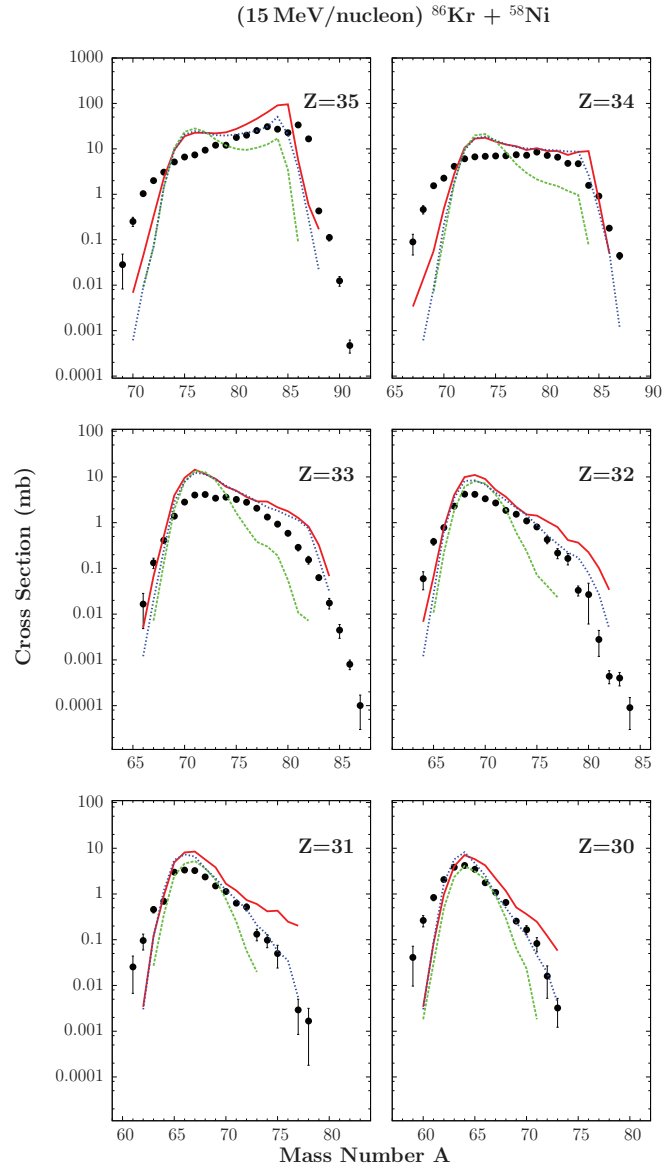

FIG. 6. (Color online) Comparison calculated mass distributions (lines) of projectilelike fragments with $Z = 35$–30 from the reaction ^{86}Kr(15 MeV/nucleon)+^{58}Ni with the experimental data (closed points) of Ref. [46]. The calculations are: CoMD/SMM [solid (red) line], DITm/SMM [dotted (blue) line], and DIT/SMM [dashed (green) line].

with $Z = 35$–30 from ^{86}Kr(15 MeV/nucleon)+^{58}Ni are compared to the experimental data (closed points) from Ref. [46]. An overall satisfactory agreement between the CoMD and DITm calculations and the experimental data for the whole range of the isotopes is obtained.

Furthermore, in Fig. 7, the results of the calculations CoMD/SMM [solid (red) line], DITm/SMM [dotted (blue) line], and DIT/SMM [dashed (green) line] for projectilelike fragments with $Z = 35$–30 from ^{86}Kr(15 MeV/nucleon)+^{112}Sn are compared to the experimental data [46]. Again the agreement of the CoMD and DITm calculations with the experimental data is reasonable. The discrepancies for nuclides with $Z = 35$ and $A = 83$–86 are due to the issues of elastic scattering contamination, as explained before for $Z = 35$ from ^{86}Kr +^{124} Sn (Fig. 5).

D. Reaction ^{86}Kr(25 MeV/nucleon)+^{124}Sn

After the comparison of calculations with the data from the 15 MeV/nucleon ^{86}Kr-induced reactions, we proceed to show representative results of CoMD, DITm, and DIT at 25 MeV/nucleon for the reaction ^{86}Kr + ^{124}Sn and compare them with the experimental data reported in our article [40]. In Fig. 8, the experimental mass distributions of projectilelike fragments with $Z = 35$–30 from ^{86}Kr(15 MeV/nucleon)+^{124}Sn [46] are compared to the results

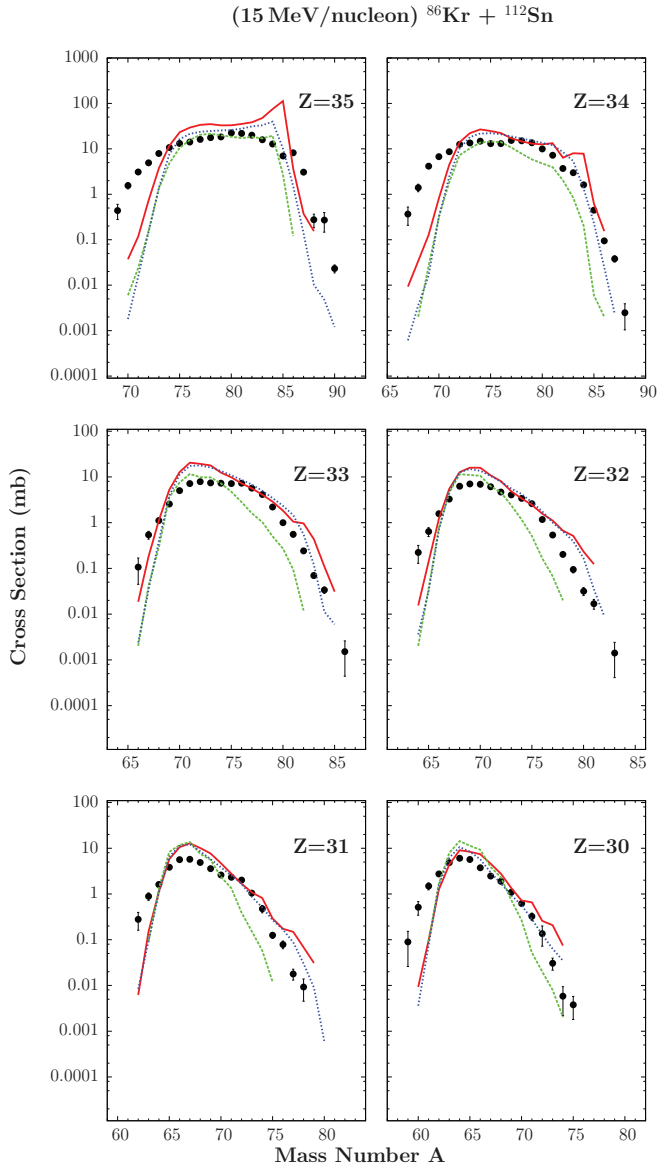

FIG. 7. (Color online) Comparison of calculated mass distributions (lines) of projectilelike fragments with $Z = 35$–30 from the reaction ^{86}Kr(15 MeV/nucleon)+^{112}Sn with the experimental data (closed points) of Ref. [46]. The calculations are: CoMD/SMM [solid (red) line], DITm/SMM [dotted (blue) line], and DIT/SMM [dashed (green) line].

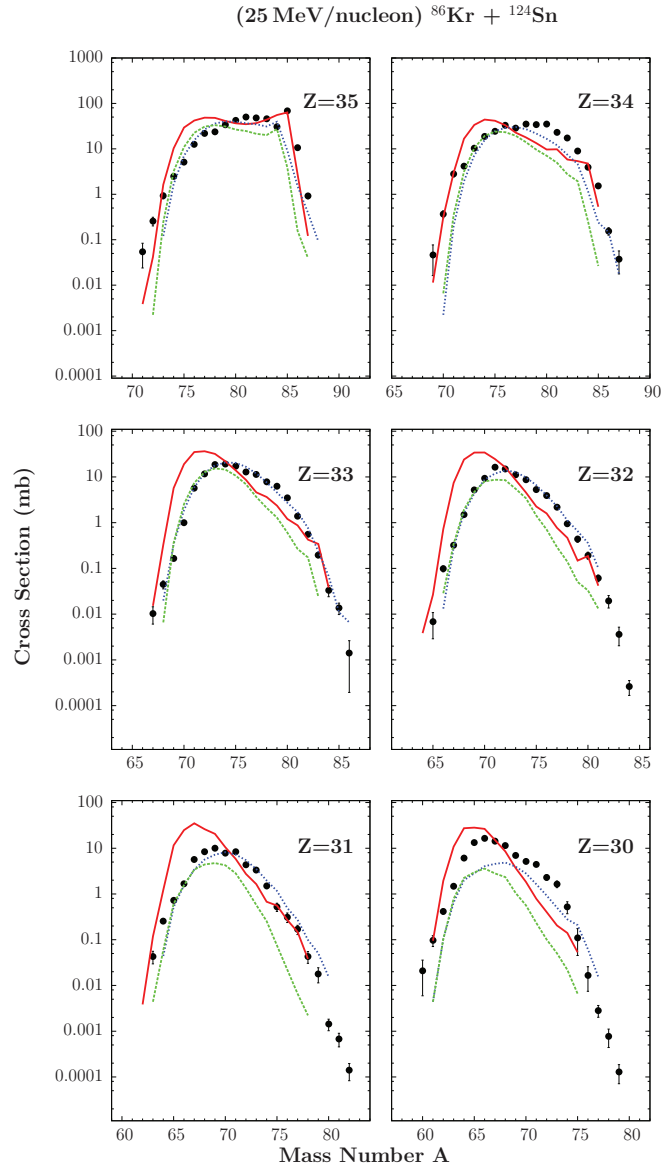

FIG. 8. (Color online) Comparison of calculated mass distributions (lines) of projectilelike fragments with $Z = 35$–30 from the reaction ^{86}Kr(25 MeV/nucleon)+^{124}Sn with the experimental data (closed points) of Ref. [40]. The calculations are: CoMD/SMM [solid (red) line], DITm/SMM [dotted (blue) line], and DIT/SMM [dashed (green) line].

of the CoMD/SMM [solid (red) line], DITm/SMM [dotted (blue) line], and DIT/SMM [dashed (green) line]. As in the corresponding reaction at 15 MeV/nucleon (Fig. 5), whereas the standard DIT does not perform well on the neutron-rich side (see also Refs. [39,40]), DITm provides reasonable results essentially for all the isotopes shown. Furthermore, we observe a fair agreement of the CoMD/SMM calculations with the experimental data on the neutron-rich side for isotopes close to the projectile. However, the CoMD/SMM calculation leads to an overestimation of the proton-rich products further from the projectile. This issue may require further investigation, but we understand that it is related to the details of the SMM deexcitation and the adopted threshold of multifragment emission (multifragmentation) that starts to appear in semiperipheral collisions at 25 MeV/nucleon [70]. Closing the discussion at 25 MeV/nucleon, we mention that for the reactions ^{86}Kr(25 MeV/nucleon)+^{112}Sn [40] and ^{86}Kr(25 MeV/nucleon)+^{64}Ni [39], our calculations lead to results of essentially similar quality to the ones shown in Fig. 8 and are not presented in this paper.

E. Radioactive beam reaction ^{92}Kr (15 MeV/nucleon)+^{64}Ni

After the preceding comparison of the calculations with the ^{86}Kr experimental data, we examine the predictions of our

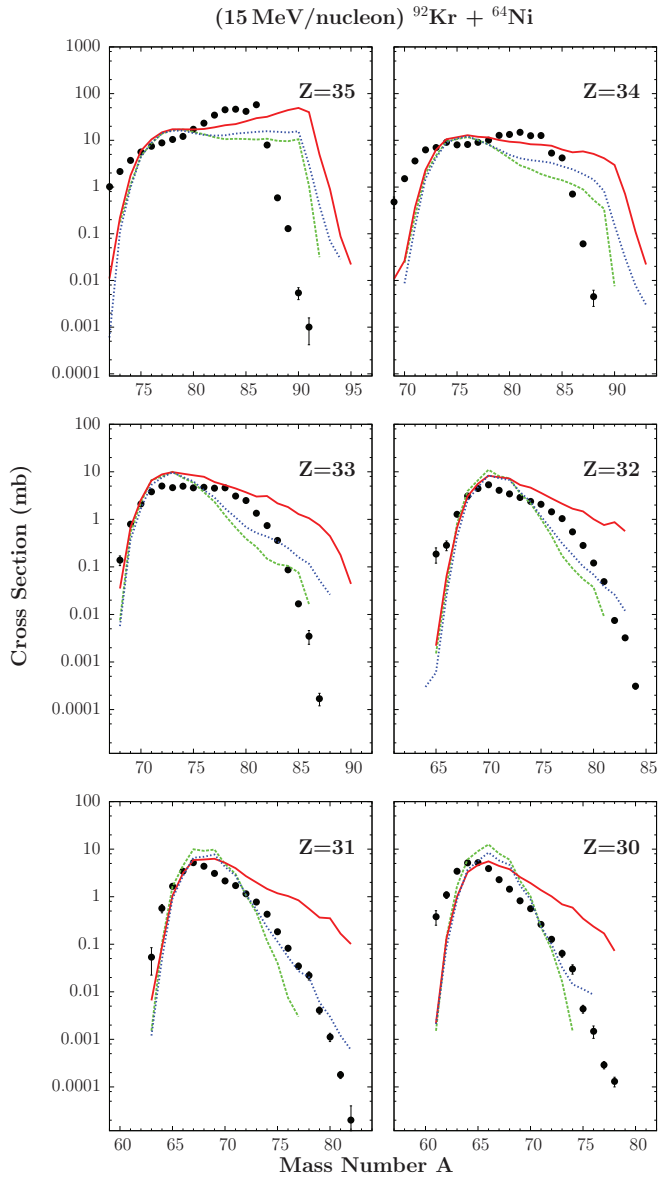

FIG. 9. (Color online) Calculations of mass distributions (cross sections) with CoMD/SMM [solid (red) line], DITm/SMM [dotted (blue) line] and DIT/SMM [dashed (green) line] of projectilelike fragments with $Z = 35$–30 from the radioactive-beam reaction ^{92}Kr(15 MeV/nucleon)+^{64}Ni. For reference displayed are the experimental data (closed points) for the stable-beam reaction ^{86}Kr(15 MeV/nucleon)+^{64}Ni [46].

model frameworks applied to a reaction induced by a neutron-rich radioactive beam, such as ^{92}Kr. In Fig. 9, for reference we present again the experimental mass distributions (closed symbols) of nuclides from ^{86}Kr(15 MeV/nucleon)+^{64}Ni. Furthermore, we show the calculations CoMD/SMM [solid (red) line], DITm/SMM [dotted (blue) line], and DIT/SMM [dashed (green) line] for the radioactive-beam reaction ^{92}Kr(15 MeV/nucleon)+^{64}Ni. From the CoMD/SMM calculations, we observe that by using the neutron-rich radioactive beam of ^{92}Kr at 15 MeV/nucleon, we can obtain neutron-rich products with several more neutrons produced with approximately the same cross section as the corresponding products with the stable beam of ^{86}Kr. It is interesting to notice that, e.g., for bromine ($Z = 35$), nuclides that have up to 14 more neutrons than the corresponding stable isotope ($A = 81$) may be produced in the radioactive-beam reaction.

We also observe that with the present implementation of the modified DIT code (DITm) [45], the predictions are below those of CoMD for the near projectile products. (Of course, as it has been the case for the DIT calculations with the stable ^{86}Kr beam, its predictions are systematically below those of DITm.) Further exploration of the DITm parameters may be necessary to make DITm agree with CoMD, (as was the case for near-projectile n-rich products), the under the assumption that the CoMD predictions are reliable. However, effects of the density dependence of the nuclear symmetry potential may manifest themselves in the CoMD calculations of peripheral collisions with the very neutron-rich nucleus ^{92}Kr, an issue that could be carefully investigated in future research. From a practical standpoint, we note that the DIT code and its modified version are rather fast (in contrast to the computer-intensive CoMD code) and thus, can be used effectively for the design of experiments with radioactive beams. This argument motivates further efforts for improvement that are subjects for future research. Of course, the ultimate benchmarking of the codes will be when the possibility opens up to obtain experimental data using radioactive beams at this energy in the future [72].

Nevertheless, we should note that in the radioactive-beam reaction, the enhanced production of the very neutron-rich nuclides appears mainly for the isotopes that are close to the projectile and diminishes for products further away from it, approaching the production from the corresponding stable-beam reaction.

A comprehensive presentation of the CoMD/SMM calculated production cross sections of the projectilelike fragments from the above radioactive-beam reaction on the Z vs N plane is given in Fig. 10. In this figure, stable isotopes are represented by closed squares, whereas fragments obtained by the radioactive-beam reaction are given by the open circles (with sizes corresponding to cross-section ranges according to the figure key). The dashed (green) line gives the location of the neutron drip line and the full (red) line indicates the expected path of the astrophysical rapid neutron-capture process (r process), as calculated in Ref. [61]. In the figure we clearly observe that the neutron pickup products from the ^{92}Kr projectile reach and even exceed the path of the r process near $Z = 30$–36.

To estimate expected production rates from the above reaction, in Table I we show, along with the predicted cross-sections, the production rates of neutron-rich projectilelike fragments assuming a ^{92}Kr beam with intensity 0.5 pnA (3×10^9 particles/sec) interacting with a ^{64}Ni target of 20 mg/cm^2 thickness. From this table, we see that it is possible to obtain useful rates of extremely neutron-rich isotopes that can be employed in a variety of nuclear structure and/or nuclear dynamics studies.

Motivated by the present results, we suggest that by using neutron-rich radioactive beams and through the mechanism of multinucleon transfer in peripheral heavy-ion collisions at these energies, we can produce very neutron-rich nuclides

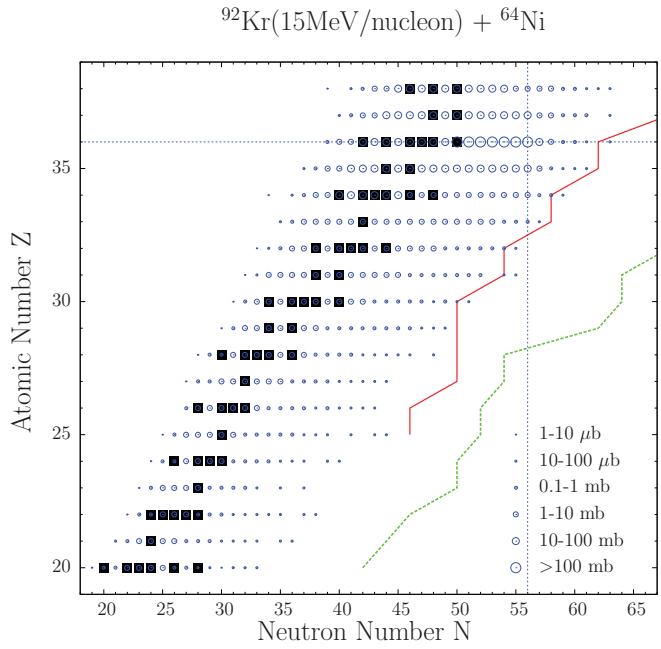

FIG. 10. (Color online) Representation of CoMD/SMM calculated production cross sections of projectile fragments from the radioactive-beam reaction ^{92}Kr (15 MeV/nucleon)+^{64}Ni on the Z-N plane. The cross section ranges are shown by open circles according to the key. The closed squares show the stable isotopes. The solid (red) line shows the astrophysical r-process path and the dashed (green) line shows the location of the neutron drip line [61]. The horizontal and vertical dashed lines indicate, respectively, the proton and neutron number of the ^{92}Kr projectile.

toward the neutron drip line. From Fig. 10, we speculate that by using neutron-rich radioactive beams below Zn ($Z = 30$), we may have the opportunity to reach the neutron-drip line for isotopes around and below Ni ($Z = 28$). We are currently exploring this possibility with our model framework. In addition, we plan to perform systematic calculations of production cross sections and rates employing a wide range of possible reaccelerated neutron-rich radioactive beams of adequate intensity in this energy range (15–25 MeV/nucleon) in order to assess the possibilities offered by our proposed approach in upcoming rare-isotope beam facilities (e.g., [26,50,72]).

TABLE I. Calculated cross sections (with CoMD/SMM) and rates of very neutron-rich isotopes from the radioactive-beam reaction ^{92}Kr (15 MeV/nucleon)+^{64}Ni. For the rates, the cross section calculations are used, and a radioactive beam of ^{92}Kr with intensity 0.5 pnA (3×10^9 particles/sec) is assumed to interact with a ^{64}Ni target of 20 mg/cm^2 thickness (see text).

Rare Isotope	Reaction Channel	Cross Section (mb)	Rate (sec^{-1})
^{93}Kr	$-0p+1n$	18.8	8.6×10^3
^{94}Kr	$-0p+2n$	2.3	1.2×10^3
^{95}Kr	$-0p+3n$	0.63	3.0×10^2
^{96}Kr	$-0p+4n$	0.2	60
^{92}Br	$-1p+1n$	4.5	2.3×10^3
^{93}Br	$-1p+2n$	0.75	4.2×10^2
^{94}Br	$-1p+3n$	0.078	40
^{95}Br	$-1p+4n$	0.039	10
^{90}Se	$-2p+0n$	2.7	1.4×10^3
^{91}Se	$-2p+1n$	0.6	3.5×10^2
^{92}Se	$-2p+2n$	0.12	60
^{93}Se	$-2p+3n$	0.039	10

V. DISCUSSION AND CONCLUSIONS

Summarizing, we presented detailed calculations of the production cross sections of projectilelike fragments produced in peripheral heavy-ion collisions of a ^{86}Kr beam at energies 15 and 25 MeV/nucleon. Specifically, we showed results for the following reactions: ^{86}Kr(15 MeV/nucleon)+^{64,58}Ni, ^{86}Kr(15 MeV/nucleon)+^{124,112}Sn, and ^{86}Kr(25 MeV/nucleon)+^{124}Sn. We presented, first, calculations with the microscopic CoMD model combined with the deexcitation code SMM (as well as GEMINI that lead to nearly similar results). In parallel, we showed calculations using the phenomenological DIT model and the modified version DITm. The latter code was able to adequately describe the neutron-rich products.

We point out that in this work, the CoMD code was employed for the first time for detailed description of projectilelike fragments from peripheral heavy-ion collisions with emphasis toward exotic neutron-rich nuclides. Our study indicated that the CoMD code, with its standard set of parameters [57,62] can describe reasonably well the multineutron pick-up products close to the projectile. The good description of the cross sections of nuclides that capture up to 6–8 neutrons from target nucleus is very important and exciting. We believe that the successful description of the production of neutron-rich isotopes with the CoMD model is especially valuable due to the predictive power of this microscopic many-body approach, which does not depend on the reaction dynamics, and thus it may be applied with some confidence to the case of heavy-ion reactions induced by rare isotope beams. In parallel, the phenomenological DITm approach can be practical for the design of experiments with rare-isotope beams at this energy. From the present systematic comparisons, we are led to the suggestion that peripheral heavy-ion collisions at energies well above the Coulomb barrier but below the Fermi energy, if induced by neutron-rich radioactive beams of adequate intensity, soon to be available in several RIB facilities worldwide, will offer a novel approach to access extremely neutron-rich rare isotopes in unexplored regions of the nuclear chart toward the neutron drip line.

ACKNOWLEDGMENTS

We are thankful to L. Tassan-Got for the DIT code, to M. Papa for his version of the CoMD code, R. Charity for the GEMINI code, and A. Botvina for the SMM code. We thank S. Galanopoulos, Z. Kohley, A. L. Keksis, B. C. Stein, and S. J. Yennello for the help and support in our previous experimental work on rare isotope production at 15–25 MeV/nucleon at the Cyclotron Institute of Texas A&M University. Finally, we wish

to acknowledge the motivation and recent discussions with Y.K. Kwon, K. Tshoo, and other members of the KOBRA team of RISP. Financial support for this work was provided, in part, by ELKE Research Account No 70/4/11395 of the National and Kapodistrian University of Athens. M.V. was supported by the Slovak Scientific Grant Agency under Contracts No. 2/0105/11 and No. 2/0121/14 and by the Slovak Research and Development Agency under Contract No. APVV-0177-11.

[1] M. Thoennessen, Rep. Prog. Phys. **76**, 056301 (2013).
[2] M. Thoennessen and B. Sherrill, Nature (London) **473**, 25 (2011).
[3] J. Erler, N. Birge, M. Kortelainen, W. Nazarewicz, E. Olsen, A. Perhac, and M. Stoitsov, Nature (London) **486**, 509 (2012).
[4] Y. Blumenfeld, T. Nilsson, and P. V. Duppen, Phys. Scr. T **152**, 014023 (2013).
[5] J. Äystö, W. Nazarewicz, M. Pfützner, and C. Signorini, *Proceedings of the Fifth International Conference on Exotic Nuclei and Atomic Masses (ENAM'08), Ryn, Poland, September 7–13* (Springer, 2008) [Eur. Phys. J. A **42**, 299 (2009)].
[6] C. Sneden and J. J. Cowan, Science **299**, 70 (2003).
[7] K. Langanke and M. Wiescher, Rep. Prog. Phys. **64**, 1657 (2001).
[8] H.-T. Janka, K. Langanke, A. Marek, G. Martínez-Pinedo, and B. Müller, Phys. Rep. **442**, 38 (2007).
[9] P. Danielewicz, R. Lacey, and W. G. Lynch, Science **298**, 1592 (2002).
[10] B.-A. Li, L. W. Chen, and C. M. Ko, Phys. Rep. **464**, 113 (2008).
[11] D. V. Shetty, S. J. Yennello, and G. A. Souliotis, Phys. Rev. C **76**, 024606 (2007).
[12] V. Baran *et al.*, Phys. Rep. **410**, 335 (2005).
[13] G. Giuliani, H. Zheng, and A. Bonasera, Prog. Part. Nucl. Phys. **76**, 116 (2014).
[14] A. R. Raduta and F. Gulminelli, Phys. Rev. C **82**, 065801 (2010).
[15] C. J. Pethick and D. G. Ravenhall, Ann. Rev. Nucl. Part. Sci. **45**, 429 (1995).
[16] J. M. Lattimer and M. Prakash, Phys. Rep. **442**, 109 (2007).
[17] *Scientific Opportunities with a Rare-Isotope Facility in the United States* (National Academies Press, Washington DC, 2007).
[18] D. F. Geesaman, C. K. Gelbke, R. V. F. Janssens, and B. M. Sherrill, Annu. Rev. Nucl. Part. Sci. **56**, 53 (2006).
[19] FRIB main page: https://www.frib.msu.edu
[20] GANIL main page: https://www.ganil.fr
[21] GSI main page: https://www.gsi.de
[22] RIBF main page: https://www.rarf.riken.go.jp/Eng/facilities/RIBF.html
[23] ATLAS main page: https://www.phy.anl.gov/atlas/facility/index.html
[24] EURISOL main page: https://www.eurisol.org
[25] K. Schmidt, A. Kelić, S. Lukić, M. Ricciardi, and M. Veselsky, Phys. Rev. Special Topics, Accelerators and Beams **10**, 014701 (2007).
[26] RISP main page: https://www.risp.re.kr/eng/pMainPage.do
[27] H. Geissel and G. Munzenberg, Ann. Rev. Nucl. Part. Sci. **45**, 163 (1995).
[28] A. Kelić, M. V. Ricciardi, and K. H. Schmidt, Bulgarian Nuclear Society Transactions **13**, 98 (2009).
[29] H. Alvarez-Pol *et al.*, Phys. Rev. C **82**, 041602 (2010).
[30] J. Kurcewicz *et al.*, Phys. Lett. B **717**, 371 (2012).
[31] H. Watanabe *et al.*, Phys. Rev. Lett. **111**, 152501 (2013).
[32] O. B. Tarasov *et al.*, Phys. Rev. C **80**, 034609 (2009).
[33] S. Lukyanov *et al.*, Phys. Rev. C **80**, 014609 (2009).
[34] O. B. Tarasov *et al.*, Phys. Rev. C **87**, 054612 (2013).
[35] C. Mazzocchi, R. Surman, R. Grzywacz *et al.*, Phys. Rev. C **88**, 064320 (2013).
[36] T. Kurtukian-Nieto, J. Benlliure, K. H. Schmidt *et al.*, Phys. Rev. C **89**, 024616 (2014).
[37] V. V. Volkov, Phys. Rep. **44**, 93 (1978).
[38] L. Corradi, G. Pollarolo, and S. Szilner, J. Phys. G **36**, 113101 (2009).
[39] G. A. Souliotis *et al.*, Phys. Lett. B **543**, 163 (2002).
[40] G. A. Souliotis *et al.*, Phys. Rev. Lett. **91**, 022701 (2003).
[41] G. A. Souliotis *et al.*, Nucl. Instrum. Methods Phys. Res. B **204**, 166 (2003).
[42] G. A. Souliotis *et al.*, Nucl. Instrum. Methods Phys. Res. B **266**, 4692 (2008).
[43] H. Fuchs and K. Möhring, Rep. Prog. Phys. **57**, 231 (1994).
[44] L. Tassan-Got and C. Stefan, Nucl. Phys. A **524**, 121 (1991).
[45] M. Veselsky and G. A. Souliotis, Nucl. Phys. A **765**, 252 (2006).
[46] G. A. Souliotis *et al.*, Phys. Rev. C **84**, 064607 (2011).
[47] G. A. Souliotis *et al.*, Nucl. Instrum. Methods Phys. Res. B **266**, 4213 (2008).
[48] A. Druart *et al.*, Nucl. Instrum. Methods Phys. Res. B **266**, 4162 (2008).
[49] J. Dvorak *et al.*, Nucl. Instrum. Methods Phys. Res. A **652**, 687 (2011).
[50] K. Tshoo, Y. K. Kim, Y. K. Kwon *et al.*, Nucl. Instrum. Methods Phys. Res. B **317**, 242 (2013).
[51] R. E. Tribble, R. H. Burch, and C. A. Gagliardi, Nucl. Instr. and Meth. A **285**, 441 (1989).
[52] M. Veselsky *et al.*, Phys. Rev. C **62**, 064613 (2000).
[53] M. Veselsky *et al.*, Nucl. Phys. A **705**, 193 (2002).
[54] M. Veselsky *et al.*, Nucl. Phys. A **724**, 431 (2003).
[55] A. L. Keksis *et al.*, Phys. Rev. C **81**, 054602 (2010).
[56] M. Veselsky and G. A. Souliotis, Nucl. Phys. A **872**, 1 (2011).
[57] M. Papa, T. Maruyama, and A. Bonasera, Phys. Rev. C **64**, 024612 (2001).
[58] M. Papa *et al.*, J. Comp. Phys. **208**, 403 (2005).
[59] J. Aichelin, Phys. Rep. **202**, 233 (1991).
[60] M. Papa, Phys. Rev. C **87**, 014001 (2013).
[61] P. Moller, J. R. Nix, and K. L. Kratz, At. Data Nucl. Data Tables **66**, 131 (1997).
[62] G. A. Souliotis, J. Phys. Conf. Series **205**, 012019 (2010).
[63] R. Charity *et al.*, Nucl. Phys. A **483**, 371 (1988).
[64] J. Bondorf *et al.*, Phys. Rep. **257**, 133 (1995).
[65] R. J. Charity, Phys. Rev. C **58**, 1073 (1998).
[66] L. G. Moretto, Nucl. Phys. A **247**, 211 (1975).
[67] J. Lestone, Phys. Rev. C **52**, 1118 (1995).
[68] A. S. Botvina and I. N. Mishustin, Phys. Rev. C **63**, 061601 (2001).
[69] N. Buyukcizmeci, R. Ogul, and A. S. Botvina, Eur. Phys. J. A **25**, 57 (2005).
[70] G. A. Souliotis, A. S. Botvina, D. V. Shetty, A. L. Keksis, M. Jandel, M. Veselsky, S. J. Yennello, Phys. Rev. C **75**, 011601 (2007).
[71] K. Sekizawa and K. Yabana, Phys. Rev. C **88**, 014614 (2013).
[72] Y. K. Kwon and K. Tshoo (private communication).